STAG: Smart Tools and Applications in Graphics (2023)
K. Lupinetti, F. Banterle, N. Capece, and U. Erra (Editors)

# Computational design of fabricable geometric patterns

E. Scandurra[1,2], Francesco Laccone[1], Luigi Malomo[1], Marco Callieri[1], Paolo Cignoni[1] and Daniela Giorgi[1]

[1] Institute of Information Science and Technologies, National Research Council of Italy, Pisa, Italy
[2] Department of Computer Science, University of Pisa, Italy

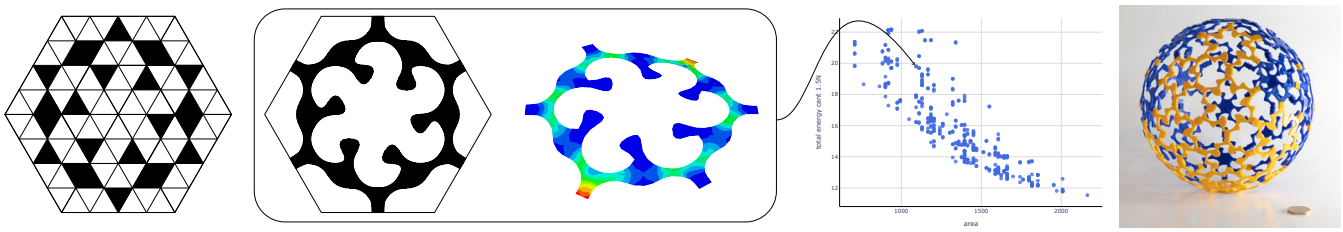


(a) (b) (c) (d) (e)

**Figure 1:** *Our pipeline, from pattern design to simulation and fabrication: (a) a polygonal pattern as a geometric configuration produced via regular recursive subdivision of the planar space, with black indicating solid material and white indicating void; (b) the corresponding fabricable pattern geometry after a refinement step; (c) the bending of the pattern under a simulated loading scenario; (d) the dot corresponding to the pattern in the browsing interface; (e) a sphere fabricated with two different patterns.*

**Abstract**

*This paper addresses the design of surfaces as assemblies of geometric patterns with predictable performance in response to mechanical stimuli. We design a family of tileable and fabricable patterns represented as triangle meshes, which can be assembled for creating surface tessellations. First, a regular recursive subdivision of the planar space generates different geometric configurations for candidate patterns, having interesting and varied aesthetic properties. Then, a refinement step addresses manufacturability by solving for non-manifold configurations and sharp angles which would produce disconnected or fragile patterns. We simulate our patterns to evaluate their mechanical response when loaded in different scenarios targeting out-of-plane bending. Through a simple browsing interface, we show that our patterns span a variety of different bending behaviors. The result is a library of patterns with varied aesthetics and predefined mechanical behavior, to use for the direct design of mechanical metamaterials. To assess the feasibility of our approach, we show a pair of fabricated 3D objects with different curvatures.*

**CCS Concepts**

• ***Computing methodologies*** → ***Computer Graphics;***

## 1. Introduction

Computational fabrication investigates the design and production of objects at different scales – from architecture to automotive and furniture – with the aim of speeding up the classic design pipeline and overcoming material, size and geometric limitations. One of the opportunities opened up by computational fabrication is the design of *mechanical metamaterials* [BBO*10, PZM*15], a class of man-made structures whose mechanical properties are determined by the structure geometry. Metamaterials can be created using *patterns*, i.e. portions of space with a unique distribution of solid material and voids. Indeed, patterns can be assembled to create tiled surfaces, and the tiling of patterns with different geometries enables controlling the mechanical behavior of the resulting surface in response to mechanical stimuli e.g. force, deformation, momentum [MSS*19]. An additional effect of pattern diversity is the creation of aesthetically pleasant surfaces; indeed, patterns have been extensively used in art and architecture for their aesthetic properties, for example for the façades of MuCEM or Texoversum and the roof of Louvre Abu Dhabi.

This paper aims at supporting the creation of metamaterials by



DOI: 10.2312/stag.20231297

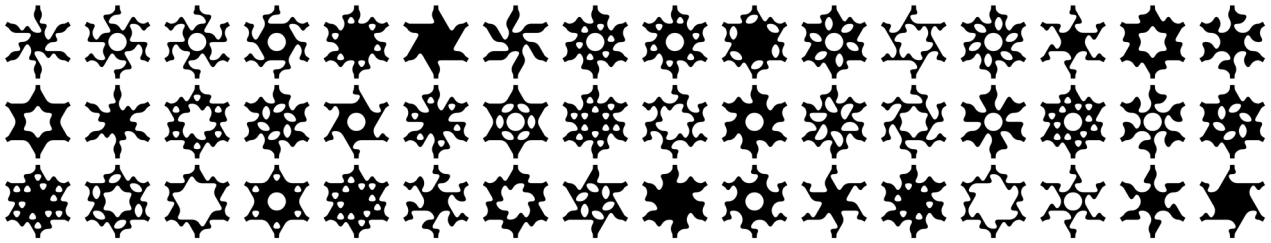

**Figure 2:** *A small subset of the family of exchangeable, tileable, and connected patterns in our family.*

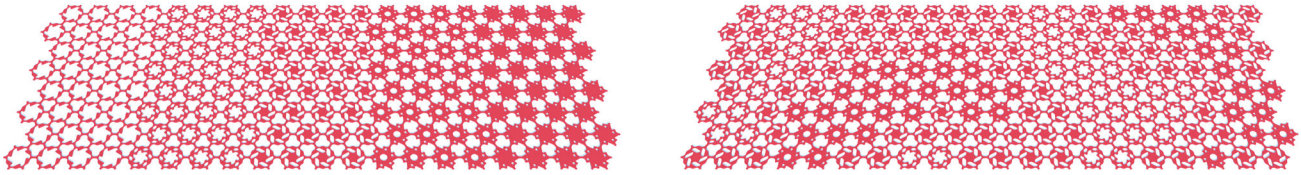

**Figure 3:** *Two example surface tessellations with different patterns.*

tiling polygonal patterns. We address the first step of the pipeline, namely the design and characterization of a family of geometric patterns that span a wide range of mechanical properties. These patterns can be manufactured by 3D printing or laser-cutting and assembled to create aesthetically-pleasing surface tilings.

We cast pattern design as the combinatorial problem of locating solid material and voids over a surface. First, a regular recursive subdivision of the planar space generates different geometric configurations (Figure 1(a)); then, a refinement step guarantees that patterns are fabricable and robust (Figure 1(b)). We simulate the patterns to characterize their mechanical response under load (Figure 1(c)), and present a simple browsing interface for exploring the design space, in terms of both aesthetics and behavior (Figure 1(d)). Differently from the majority of existing works, we target out-of-plane 3D deformations, and evaluate the bending response of patterns in three different scenarios. Our simulation results show that the patterns exhibit a range of different mechanical properties, and greatly expand the spectrum of possible deformations when compared to solid structures. The user can select a pattern based on the desired stiffness and target deformation. Finally, different patterns can be easily manufactured as flat pieces and then assembled to form spatial assemblies (Figure 1(e)).

Our result is a library of patterns that can be employed to create surface tessellations for the direct design of metamaterials. Figure 2 shows some example patterns, which span a variety of geometric and aesthetic properties. In turn, Figure 3 shows example surfaces produced by assembling subset of patterns in different configurations: adjacent patterns blend smoothly, and the whole metamaterial sheet has a seamless appearance.

Our contribution is a simple yet elegant method to produce aesthetically pleasant patterns at a controllable scale, for the direct design of mechanical metamaterials.

## 2. State of the art

Metamaterials are man-made structures for which the specific internal organization of elements achieves some required behavior in terms of deformation, stress or energy [MLC*22, BSP19, MSS*19, YZL*18]. Metamaterials are often created as tilings of patterns [DLL*15, MDLW15]. Patterns are sensible as target geometries are often not reproducible in the real world due to material or manufacturing constraints, and need to be decomposed or simplified.

Polygonal tilings have been studied for a long time in mathematics [Kap09, GS87]. Several works use ornamental patterns to approximate a desired 3D shape with discrete tiles [ZJL14, ZCT16, CML*17]. Patterns have been also used to realize *stylized surfaces* [BCMP18], geometries that follow the shape of a target object at its macro-scale, while at a lower meso-scale they present distinctive geometrical, physical, structural, and appearance properties. Stylized surfaces are gaining momentum in architecture: an example is the FlexMap Pavilion, whose constituent elements are spirals, and which was shown at the Venice Architecture Biennale in 2021 [LMC*22].

Our problem also relates to *topology optimization* methods, which investigate the problem of optimally distributing solid material within a target volume [SM13]. Topology optimization methods are able to create efficient patterns by volume subtraction and model update, leaving the material only where needed. However, only a specific mechanical task can be satisfied at a time, and steady-state loading conditions are usually employed. Instead, we target nonlinear conditions and multiple scenarios to provide a repository for the user to browse.

Our method deals with generating flat patterns tiled on a surface. Flat pieces are practical since they can be easily transported and manufactured in different sizes with different fabrication techniques. [MPI*18] approximates an input surface using flat pa-

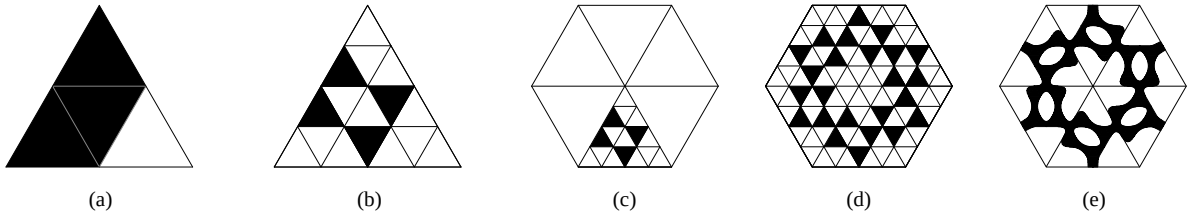


**Figure 4:** *The steps in our pipeline. We consider different configurations of solid/void subtriangles in a triangular slice, at multiple subdivision steps (a,b). The triangle slice is embedded into a polygon, an hexagon in this example (c). A polygonal pattern is generated by replicating the triangle slice via rotational symmetry (d). To get the final fabricable patterns, we add solid material around predefined vertices using quadratic rational Bézier curves and a connectivity-preserving logic (e).*

rameterized spiraling patterns to produce both small-scale and architectural-scale objects [LMC*22, LMP*21]. However, the pattern geometry is constrained to a four-arm spiral pattern, and the reduced representation proposed in [MPI*18] is only applicable to that specific type of pattern. In contrast, our goal is to produce a wide family of patterns, providing great variability both in aesthetics and in mechanical properties.

Tozoni et al. [TDJ*20] created a set of parametric rhombic microstructures with a continuous mapping between geometric parameters and mechanical properties. Similarly, Martinez et al. [MSS*19] generate 2D tiled geometries from Voronoi diagrams of regular lattices under star-shaped distance functions. Their microstructures can be interpolated to smoothly vary their mechanical properties. To assess the mechanical behavior of pattern arrangements, the authors relied on homogenization [KMOD09]. However, these approaches applies only to in-plane scenarios, where the patterns have few deformation modes and it is easier to map them to a simpler mechanical model. In contrast, in this work we target out-of-plane deformation of flat patterns, and we run *a posteriori* simulations so that the user can explore the space of all possible behaviors and select the most suitable pattern on the basis of its response. Indeed, homogenizing a generic 3D mechanical behavior is still an open research question [SMGT18], which is beyond the scope of this paper.

## 3. Methods

Our aim is to design patterns that can perform as building blocks in composing larger macrostructures. We assume a polygonal and as regular as possible tessellation for the target surface, in which as many tiles as possible have the same shape, for example hexagons [PTP*15].

The patterns should be *tileable*, i.e. connect properly to adjacent patterns when placed in a tile, and *exchangeable*, i.e. fit into any region of the tessellation so that they can switch place, to expand the design space of mechanical structures achievable. We start from the idea that every regular convex polygon can be decomposed into a fan of isosceles triangles emanating from its centroid; for example, a regular hexagon can be decomposed into a fan of six equilateral triangles. Therefore, we can create a polygon pattern by generating a sub-pattern of a triangular *slice*, and then replicating it by rotational symmetry to fill any convex $n$-sided polygon. To generate different triangular slice patterns, we perform a combinatorial exploration of possible designs through recursive triangle subdivisions, by considering all possible configurations of solid/void subtriangles at each subdivision step. Figure 4(a,b) shows example configurations for two subdvision steps. Once a triangular slice pattern has been designed, we generate the corresponding polygonal pattern by replicating the slice (Figure 4(c,d)). The resulting rotational symmetric *pattern* embeds into the original polygon, can be easily adapted to polygons with a different number of edges by linearly mapping the base slice into every fan triangle, and is exchangeable by definition. Moreover, due to rotational symmetry, the positioning of a pattern is independent of possible rotations: this is convenient, as the mechanical properties of a structure composed by non-symmetric patterns would depend on the direction of each metamaterial units inside the structure.

To guarantee connectedness and tileability, we define a filtering strategy to rule out slice configurations producing disconnected patterns and patterns that do not properly connect to the boundaries. Finally, the last issues to address are fabricability and suitability for simulations. Indeed, the presence of non-manifold configurations and sharp angles in the pattern geometry would lead to disconnected or fragile patterns, and possibly to singularities in computation. We address the problem by locally refining the geometry of patters using quadratic rational Bézier curves: we automatically identify problematic areas that would generate disconnected or fragile patterns, and add material to produce fabricable geometries (Figure 4(e)).

The next Sections detail the single steps of the pipeline.

### 3.1. From slices to patterns

We start by generating a geometry that can fit into any isosceles triangle (a slice). More formally, a *slice* is a regular triangulation of a base triangle; every face has a label which is either 1 or 0. Label 1 indicates solid regions (i.e. regions filled with material), while label 0 indicates void regions. Sometimes it will be useful to refer to the subcomplex generated by the solid triangles, which we will call *solid slice*.

Figure 5 illustrates the process of subdivision and slice generation. To list the set of possible triangles slices, we perform a combinatorial exploration of the space of possible slices through regular recursive subdivision of a base triangle (1 to 4). We start from the

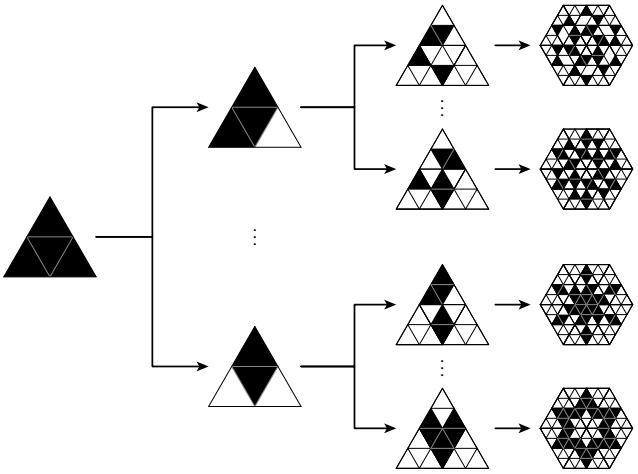

**Figure 5:** *From left to right: the solid triangle; two possible solid/void configurations produced after a first subdivision step; four possible solid/void configurations produced after a second subdivision step; the polygonal patterns they generate.*

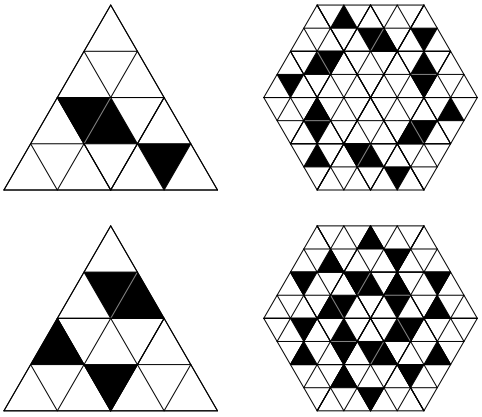

**Figure 6:** *(Top) A connected solid slice that generates a disconnected solid pattern; (bottom) a disconnected solid slice that generates a connected solid pattern.*

solid triangle, which represents the full slice (Figure 5, left), and subdivide it into four subtriangles. We then consider all possible configurations of solids/voids, adopting a subtractive approach and removing triangle areas. We exclude the all-void configuration, as we require that a solid triangle produces at least one solid subtriangle. Each slice can be visualized by coloring in black and white the solid and void subtriangles respectively. For each configuration, we further subdivide each triangle into four as above. Again, following a subtractive approach, a solid triangle will generate all but one (15) configurations of solids/voids, while void triangles produce only the void configuration (Figure 5, middle).

The process can be recursively applied, thus producing a tree of configurations. At the $n$-th step of recursion the base triangle is subdivided in $4^n$ subtriangles, with at least a solid one. This corresponds to $2^{4^n} - 1$ possible slices. In this work we consider two steps of recursion, corresponding to $2^{16} - 1$ possible slice geometries. If we define an ordering of the faces of the triangulation, we can encode the sequence of solids/voids in a bit-string that uniquely defines the slice.

Replicating a slice by rotational symmetry generates a triangulation of a regular hexagon with labeled faces (Figure 5, right). We refer to this new labeled triangulation as a *pattern*. We encode the geometry of each pattern by $V, F, c$, where $V$ is the list of vertices, $F$ is the list of triangular faces and $c$ is a binary vector of size $|F|$ expressing whether the $i$-th element maps by rotational symmetry to a solid (or void) triangle of the generating slice. In analogy to above, we call *solid pattern* the subcomplex induced by the solid triangles of a pattern. Each solid pattern is identified by a couple $\widetilde{V}, \widetilde{F}$, where $\widetilde{F}$ is the subset of $F$ determined by faces that are labeled by 1 in $c$.

### 3.2. Exchangeability, connectedness, tileability

**Exchangeability** By construction, all slices generate patterns that can be embedded into any regular polygon, hence exchangeability is guaranteed. Unfortunately, not all patterns are suitable to produce mechanical metamaterials. Indeed, triangle slices may produce solid patterns that consist of separate components; therefore, we need to select only slices that generate connected solid patterns. Furthermore, we need to ensure tileability, so that patterns that are embedded into adjacent polygons properly connect to each other. Tileability and connectedness together ensure that, if a target surface is connected, it remains connected if tessellated using any subset of patterns. The next paragraphs detail our filtering strategy to select slices that produce connected and tileable patterns.

**Connectedness** We observe that disconnected slices may produce connected patterns and vice versa, as shown in Figure 6. Therefore, studying the connectedness of a single slice is not sufficient to check that it produces a connected pattern, and we have to analyse the whole pattern. We associate the pattern with a graph $G$ that encodes adjacency between the faces of the generated solid pattern: we associate a node with each face of the triangulation representing a solid pattern (face node) and with each of its three vertices (vertex nodes); two nodes are linked by an edge if and only if one corresponds to a face and the other to one of its vertices.The graph thus defined is a connected simplicial complex of dimension 1, such that the link of a vertex-node is the discrete set of face-nodes associated to the triangles that contain that vertex. It holds that a slice produces a connected solid pattern if and only if the graph $G$ is connected. In practice, it is sufficient to build $G$ on three triangles out of six (half a pattern), up to identification of two diametrically-opposed edges.

**Tileability** Having defined a criterion to select slices that correspond to connected solid patterns, we must deal with the problem of assembling solid patterns to produce a connected structure. Patterns must connect along the boundaries of the polygon. Therefore, we need to restrict to solid patterns that touch the boundary of the polygon. Obviously, this is not a sufficient condition: if two adjacent solid patterns are connected to disjoint points on the polygon boundary, they still fail to connect to one another (Figure 7(a)). Additionally, we have to prevent patterns from only partially con-

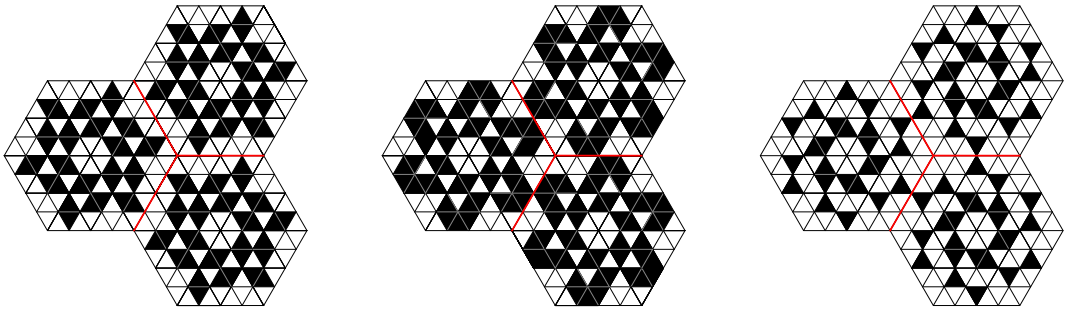


**Figure 7:** *Sample tiling of a single pattern in a hexagonal tessellation: (a) a solid pattern that fails to connect; (b) a solid pattern that fails to properly connect; (c) a solid pattern that properly connects.*

necting along the polygon boundary (Figure 7(b)), which would complexify mechanical interaction of adjacent solid patterns.

To ensure proper connection, we impose the condition that the intersection between a solid pattern and a polygon edge must be symmetric with respect to the midpoint of the polygon edge. We say that two patterns *properly connect* if they induce two solid patterns such that the edges and vertices that lie on the common polygon boundary coincide (Figure 7(c)). A family of patterns that properly connect to each other is tileable and is suited for mechanical simulations. To avoid complex behaviors in mechanical interactions of adjacent solid patterns, we restrict to patterns that connect exclusively on the open edge of the polygon, thus excluding the case of three (or more) solid patterns sharing a polygon vertex. In particular, we select solid patterns that connect to the boundary of the polygon exactly by the midpoint of its edges. To perform this selection, we simply check that all faces of the slice's boundary edge are void except the middle triangle (e.g., Figure 4(c)).

The solid patterns are then modified to produce a metamaterial that is fabricable, with a *filleting* procedure described in the next Section.

### 3.3. Filleting

Thus far we have defined conditions for slices to produce solid patterns which are tileable, exchangeable, and connected. However, to generate fabricable solid patterns with a proper structure and suited to perform mechanical simulations, we need some post-processing. Indeed, slices with non manifold vertices produce solid patterns which, when manufactured, would result in either a disconnected object or a very fragile one. Similarly, the connections between patterns should be robust enough. Finally, the presence of sharp angles can lead to inaccuracies in computation during mechanical simulation of pattern behavior, and also affect the aesthetics of patterns. Figure 8(a) shows problematic vertices in a solid pattern: non-manifold vertices (green dots), sharp angles (blue dots), and interface vertices that connect two patterns (red dots). To address these issues, we locally refine the shape of the solid pattern around problematic vertices, by adding or removing solid material, according to the configuration of the star of vertices. In other words, we edit patterns so that they are represented by a 2-dimensional piecewise-linear (PL) manifold mesh with boundary, where the boundary PL-approximates smooth curves (Figure 8(c)).

The first step is to identify problematic vertices. This can be done by analyzing the link of each vertex in a solid pattern. Non-manifold vertices are identified as vertices whose link is disconnected. Sharp angles are identified as vertices whose link is connected and made of a number of edges different than three or six. Interface vertices are identified as vertices that lie on the polygon edge. Figure 9(a,c,e,g,i,k,m) shows the set of possible configurations of solid/void triangles in the star of a non-manifold vertex, up to rotations; Figure 10(a,c,e,g) shows the set of possible configurations of solid/void triangles in the star of a vertex corresponding to a sharp angle, up to rotations. Lastly, Figure 11(a) shows the configuration for interface vertices, up to rotations.

The idea is to locally refine the mesh representing the pattern around a problematic vertex, by adding vertices in its open star. The vertices approximate quadratic rational Bézier curves, whose control polygons are pairs of edges incident to the problematic vertex, and shared by a solid and void face. The pairs of edges defining the control points are chosen so as to preserve the connectedness of the pattern. The weights for the control points are assigned by following different strategies, depending on whether the vertex lies in the interior of the polygon or on one of its edges. Therefore, we create a look-up table, with all problematic vertex configurations and the corresponding filleting strategy. If the vertex is non-manifold or it represents a sharp angle, we assign the same weight to all the control points, thus producing a quadratic Bézier curve. The resulting curves are shown in Figure 9(b,d,f,h,j,l,n) and Figure 10(b,d,f,h). If instead the vertex lies on a polygon edge, the curves are defined considering that, once the patterns are connected, the vertex produces a non-manifold configuration already considered in the previous cases (Figure 11). In this case, to produce a stiff connection among patterns, we assign different weights to the control points. In this paper, we consider $(1, 0.2, 1)$ as the weight vector for control points, where 0.2 is assigned to the interface vertex and 1 is assigned to its adjacent control points. The resulting curve is shown in Figure 11(b). This choice of weights ensures that the patterns can be simulated and properly fabricated, without their aesthetics being altered.

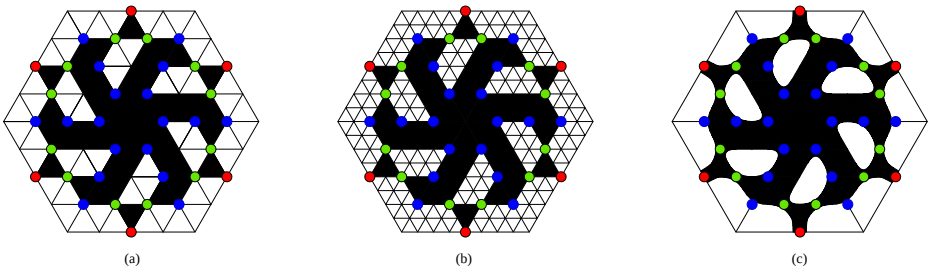


**Figure 8:** *(a) A pattern as a simplicial 2-complex with colored faces. The sub-complex generated by black faces is the solid pattern, which has non-manifold vertices (green dots), vertices identifying sharp angles (blue dots) and interface vertices connecting different patterns (red dots); (b) Mesh refinement, before the filletimg procedure around problematic vertices; (c) filleted pattern, with boundaries that approximate smooth curves.*

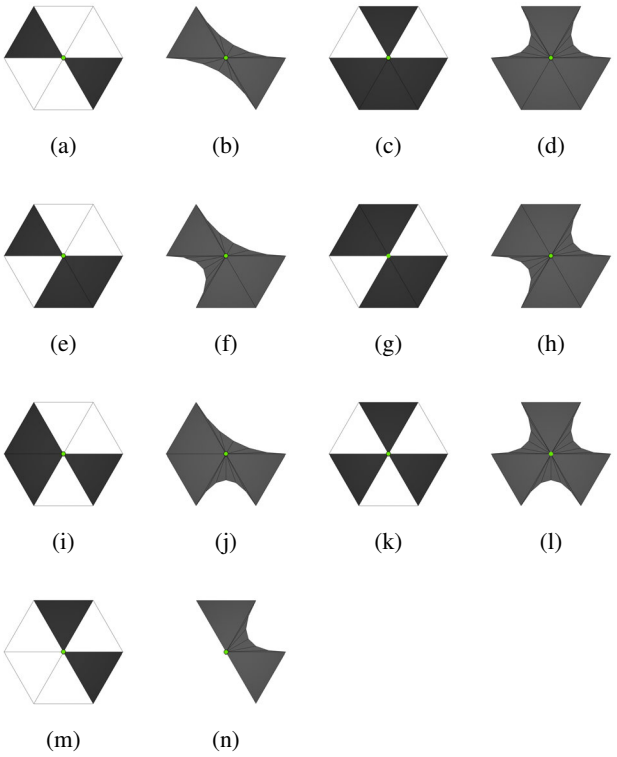


**Figure 9:** *All possible configurations of solid/void triangles in the star of non-manifold vertices (a,c,e,g,i,k,m) and the corresponding filleting strategies (b,d,f,h,j,l,n).*

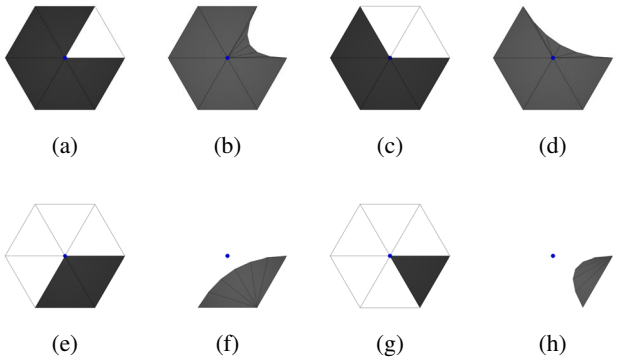


**Figure 10:** *All possible configurations of solid/void triangles in the star of vertices at sharp angles (a,c,e,g) and the corresponding filleting strategies (b,d,f,h).*


**Figure 11:** *Filleting interface vertices that lie on the polygon edge.*

One issue to solve is that different orderings in which to perform the filleting of vertices could produce different results. Indeed, the filleting would affect the star of the vertices. To this end, we perform a mesh subdivision step to guarantee that local modifications around each vertex are independent of the ordering in which they are applied. Formally, let $\mathcal{L}$ be the set of indices of problematic vertices in the mesh $\mathcal{M} = (V, F)$ representing the pattern. We perform a refinement step by further subdividing the triangles into four sub-triangles (Figure 8 (a)). This produces a new mesh $\hat{\mathcal{M}} = (\hat{V}, \hat{F})$ and a corresponding set $\hat{\mathcal{L}}$ of updated indices of vertices to process. In the refined mesh $\hat{\mathcal{M}}$, the vertices in $\hat{\mathcal{L}}$ will necessarily belong to different faces; in particular, their open stars will be pairwise disjoint. Therefore, the local modification of the open star of vertices in $\hat{\mathcal{L}}$ yields results which are independent of the ordering of vertex processing.

To locate the set of vertices $B$ approximating the boundary curves, we employ the generalized De Casteljau algorithm for rational Bézier curves [ŠJ15]. We update the set of vertices $\hat{V}$ by adding the vertices in $B$; we update the set of mesh faces $\hat{F}$ accordingly. It is important to note that, thanks to the subdivision step yielding to $\hat{M}$, the rational Bézier curves are locally defined so that geometric continuity of the tangent vector is globally ensured (Figure 8(c)). Finally, if $\widetilde{\mathcal{M}}$ is the mesh representing the solid pattern induced by

$\hat{\mathcal{M}}$, we isotropically remesh $\widetilde{\mathcal{M}}$, before simulating its mechanical behaviour.

### 3.4. Implementation details

We implemented our pipeline in Python, using the libraries IGL [JP*18] and meshplot [Seb] to manipulate and visualize 3D meshes, and numpy [HMvdW*20] to implement the algorithm for rational Bézier curves. We used the software [HDD*93] to remesh patterns before simulations, and the software Abaqus [Smi09] to perform the simulations described in the next section.

The amount of patterns that constitute the library depends on the number of subdivision steps performed in the combinatorial exploration phase. In this paper, we considered two subdivision steps: the combinatorial exploration phase produced 65535 geometries; after the filtering procedure, 430 exchangeable, connected, tileable patterns were left. Larger libraries can be obtained by performing more subdivision steps.

## 4. Simulating and navigating the design space

We consider three different loading scenarios (Cantilever, Cylinder and Dome) to characterize the mechanical response of patterns, and analyse the simulation results in detail for two different patterns (Section 4.1). Our results show that patterns exhibit diverse mechanical responses which differ from the behaviour of solid, non-patterned structures, thus expanding the range of behavior of homogeneous structures. To support the user in the navigation of the design space, we implemented a browsing interface that allows the exploration of the library of patterns in terms of mechanical properties and aesthetics (Section 4.2).

### 4.1. Structural simulations

We tested the entire dataset of patterns against three standard scenarios that cover a sufficient range of deformations. These scenarios mobilise the main ways of loading 2D plates in the out-of-plane direction, which induce 3D bending. While characterizing a mechanical metamaterial for in-plane deformation or loading is a widespread topic, exploring its bending behavior in 3D is a novel subject. We used the commercial Finite Element software Abaqus [Smi09] to deliver these simulations. Before solving the models, we remeshed the examples with an isotropic triangulation to have a good approximation of the continuum behavior. We adopt a material used for 3D printing, PLA with a density of 1.24 $g/cm^3$ and stiffness of $E = 1$ *GPa*. We used patterns installed in a regular hexagon of 3.6 *cm* edge, and a constant thickness of 0.2 *cm*. All the loading and constraints on degrees-of-freedom are applied on the pattern interface nodes only. We use shell finite elements to solve geometrically nonlinear analyses, aiming at accurately capturing their large deformation capacity. We adopted constant-load simulations, so as a result we achieve different displacements and energies because the patterns have variable stiffness. In theory, stiffer patterns result in lower strain energy, while less stiff patterns can achieve larger displacements, so they accumulate more energy. However, the geometry of the structural material play a relevant role and there are several local structural features that a pattern may exhibit.

We showcase two patterns having different geometric features and void/solid distribution to describe the three scenarios and to prove the high variability of their structural response. The first pattern has rotational symmetry and has small area located peripherally. The second pattern has XY symmetry and has dense, centered area.

In our first scenario the pattern is cantilevering from one interface extreme and is submitted to an out-of-plane force of $F_z = 1.5\,N$ on the opposite extremity. The fixed extreme has fully fixed nodes. We aim at simulating the elastica shape of the patterns. The results in Figure 12(a) show the deformed shape of the patterns in the Cantilever scenario with a superimposed color map of the strain energy per finite element. The patterns initially lay on the XY plane. As expected, even for this simple scenario the structures show a diverse and complex behavior. The first pattern (Figure 12(a,top)) has a non-symmetric deformation field and uneven distribution of stress, as demonstrated by the non-symmetric colors in the map. For a same load, it attains higher deformation than the second (Figure 12(a,bottom)). The load path from the application point to the support is long in the first case, so the stress flows along the entire pattern. Besides its larger area, the second pattern is also more efficient providing a more direct load path. Moreover, its stress and deformation is XY symmetric. A solid hexagon would behave similar to the bottom pattern, but with a stiffer response. Instead, it would be impossible to compare the top pattern with a solid hexagon, i.e. with the idea to perform homogenization.

In our second scenario (Figure 12(b)) the patterns are deformed to assume a cylindrical shape. In this setup we use pin joints on the one extreme to fix X, Y, Z translations and roller joints on the other one to fix Z translations only. Then, we applied a bending moment $M_x = -50\,Nmm$ on both the extremes to shrink the Y distance between them (the rollers slide towards the pins) while inflating the shape. The results show a different stiffness of the patterns as demonstrated by the displacement field and the strain energies. While the largest utilization of the structural material is at the supports as expected, the less dense pattern (Figure 12(b,top)) is characterized also by localized high-energy areas when the width of patterns is reduced. Instead, when the width is larger, parts of the patterns are unused and dangling, so they remain almost flat. The color map has rotational symmetry. The pattern in Figure 12(b,bottom) has a very low XY-symmetric deformation and can be compared with a solid hexagon tile.

Our third scenario simulates double curvature (Figure 12(c). Here, one extreme has pin joint (X, Y, Z fixed translations), while all the others have roller supports, so they are constrained to be on the XY plane but they can slide on it. We applied bending moments $M = 100\,Nmm$, whose axes are aligned with edge of each extreme, to have a blow-up effect that makes the shape similar to a Dome. In this scenario, bending forces applied with different axes induce a complex state of internal forces acting in the pattern. Therefore, the strain energy is affected by the straight bending along the supports and by in-plane bending elsewhere. In particular, the pattern in Figure 12(c,top) suffers from stress concentrations in the areas of small width due to in-plane bending. The patterns has a large deformation and attains high strain energy consequently. Instead, the pattern in Figure 12(c,bottom), is much more efficient because

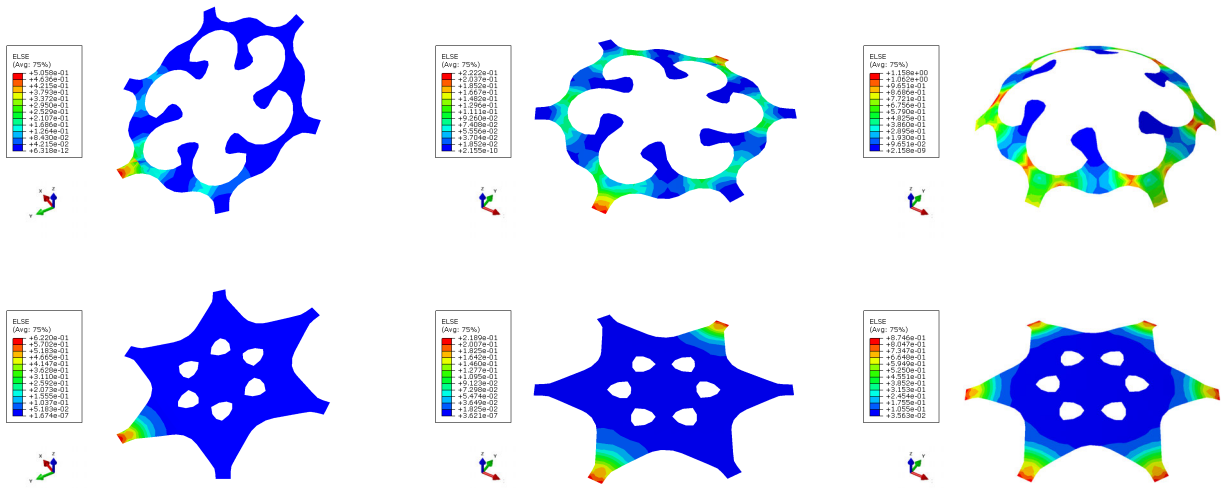

(a) (b) (c)

**Figure 12:** *Mechanical analysis results: 'Cantilever' (a), 'Cylinder' (b) and 'Dome' (c) simulation cases shown for two patterns (top and bottom). The strain energy is color-mapped on the deformed pattern.*

it has larger and centered structural material to face the equilibrium of all the radial forces coming from the extremes. Moreover, its 'star points' are affected by straight bending only.

### 4.2. Exploring the design space

From the user perspective, finding patterns that exhibit a certain aesthetics and simultaneously a target mechanical behavior is not easy, being the relation between geometry and mechanical performance often not intuitive. Therefore, we designed a simple browsing interface that enables the exploration of the design space, in terms of both aesthetics and behavior, using scatterplots. Dots in the scatterplots are patterns, while $x$ and $y$ coordinates indicate geometric and mechanical parameters (area, perimeter, and their normalized ratio, polar moment, total strain energy).

The geometric complexity of the patterns makes the mechanical characterization a hard task, since each pattern can be strongly affected by local phenomena, i.e. excessive deformation, stress concentration or even failure. Nevertheless, in the early design phase, it is convenient to describe a pattern mechanical behavior by means of a high-level single parameter, so that the user can select a subset of patterns to employ in a tiled configuration. Internal forces among patterns spread out on the basis of their stiffness, and to have equilibrium all patterns shall have a similar energy level. Therefore, we show examples of navigating the design space of our patterns while using the total strain energy of a pattern in each scenario.

Figures 13 and 14 report examples of plots that can be explored in our design interface. To describe the geometric features of the patterns we use perimeter ($mm$) and area ($mm^2$). As a consequence, clusters in the scatter plot perimeter-area highlight patters that are uniform from an aesthetic perspective. Identifying cluster is quite simple due to the discrete nature of the generation process of removing one triangle at a time. We use the polar moment of area as an additional parameter to plot the values. The polar moment has a geometric meaning and characterizes the distribution of the area with respect to the center of the hexagon. For the same area, patterns with peripheral distribution have higher polar moment. Additionally, polar moment has a mechanical meaning, in that is describes the attitude of a body to resist torsion. Moreover, polar moment is the sum of the two moments of area, namely the description of the resistance to bending. In general, the higher the polar moment, the stiffer the pattern. Finally, this parameter is quite simple to compute and can be obtained from geometry only.

In Figure 13 we select patterns from a geometric cluster. In the plots (b), (c), (d) these patterns reveal a very different mechanical behavior as shown by the colored dots in the scatter plot. The importance of the strain energy can be observed by looking at the patterns highlighted in blue and magenta: even if they have similar area, perimeter and polar moment, the second one is more efficient and do not suffer of underused parts (dangling components discussed in the previous Section).

In Figure 14 we select a different cluster of patterns having higher area and lower perimeter. Therefore they are compact and more stiff on average than the patterns in the previous cluster. The same discussion on the dispersion of energy data also holds in the present case. However, it is important to observe that the mechanical performance is also scenario-dependent. Indeed, the first pattern of the present cluster has total strain energy similar to the last pattern in the previous cluster in the case of Cantilever and Dome, while this value is different in the Cylinder scenario.

The features described above open up various possibilities to combine patterns based on the visual effect a designer may want to achieve. But they also remark the centrality of the intended use of a tessellated plane since only certain combinations of patterns

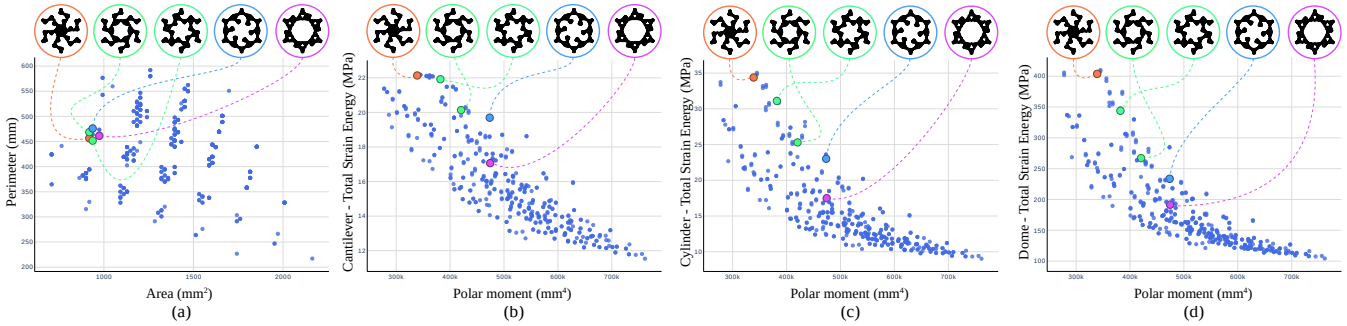


**Figure 13:** *Scatter plots representing the family of patterns and the relation between geometric and mechanical characteristics. Each dot represents a pattern. (a) A first cluster of patterns having similar geometric features, highlighted in color; scatter plot according to perimeter and area. (b,c,d) Scatter plots for the three different simulation scenarios, according to polar moment and total strain energy.*

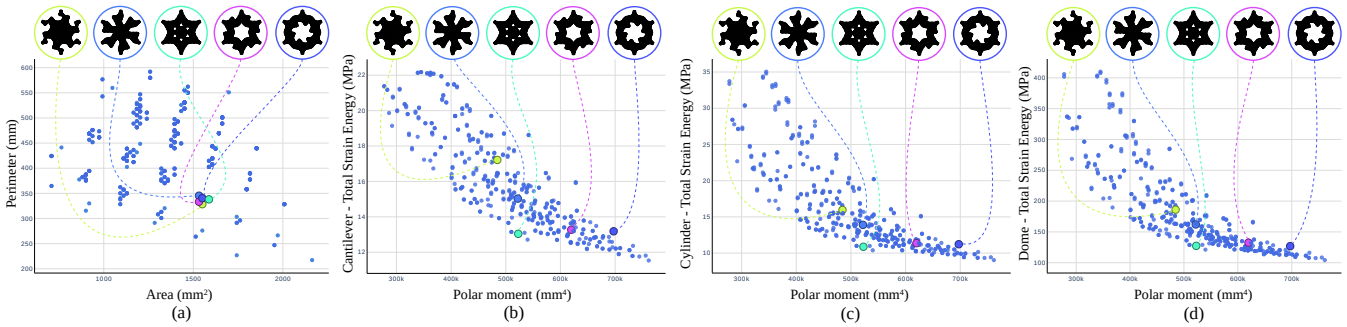


**Figure 14:** *Scatter plots representing the family of patterns and the relation between geometric and mechanical characteristics. Each dot represents a pattern. (a) A second cluster of patterns having similar geometric features, highlighted in color; scatter plot according to perimeter and area. (b,c,d) Scatter plots for the three different simulation scenarios, according to polar moment and total strain energy.*

are effective for a given curvature or target shape, as shown by the fabricated examples in the next Section.

## 5. Fabrication results

Our patterns can be assembled to create diverse surface tessellations. In a direct design fashion, the patterns can be selected from the design interface based on their aesthetics and stiffness. The pattern stiffness is related to its strain energy: since our simulations use a constant force for all patterns in a scenario, patterns with a smaller resulting strain energy are stiffer than patterns with a higher one. The latter have larger deformation.

Recently built examples [MPI*18, LMC*22] demonstrate that, when joining patterns with uniform stiffness, both the tributary internal energy and deformation are similar; instead, when joining patterns with different stiffness, only the tributary internal energy is similar. To showcase this effect, we cherry-picked 5 patterns from the scatter plot of the cylinder scenario having well distanced strain energies. In our specimen in Figure 15 (left) we tile groups of six regular hexagons to form a patterned strip and we provide pin restraints at the extreme to observe a cylinder-like deformation. As expected, the internal strain energy is constant for equilibrium reasons, and consequently stiffer patterns (on the right) are almost undeformed. The bending attitude grows moving to the left as the groups of patterns are ordered from the stiffer to the softer. The result is a surface which bends asymmetrically. The 3D printed flat PLA patterns are regular hexagons of 3.6 *cm* edge and 0.2 *cm* thickness, i.e. having same properties adopted for the simulations. All patterns interfaces are connected through a 3D printed sleeve providing full restraint, so that the resulting deformation of the assembled specimen is uniquely provided by the patterns' bending capacity.

Another fabricated specimen is shown in Figure 15 (right). We adopted a truncated icosahedron geometry made of 20 regular hexagons and 12 regular pentagons to form a spherical surface. The purpose is demonstrating the validity of our approach in the generation of patterns for different polygons and their tileability property. In general, if the polygon is as regular as possible, the structural simulations are valid in relative terms even if the number of polygon edges changes. Therefore, the use of different polygons as singularities has a negligible effect on the overall shape. In the present case, we selected two patterns from the dome scenario with similar strain energy producing indeed, when jointed, a spherical shape without distortions. It is worth mentioning that the adopted geometry and the number of connections favorably introduce a strong geometric constrain. The patterns have a negligible in-plane strain and all the deformation is necessarily achieved by bending.

The seamless transition between the different patterns in the

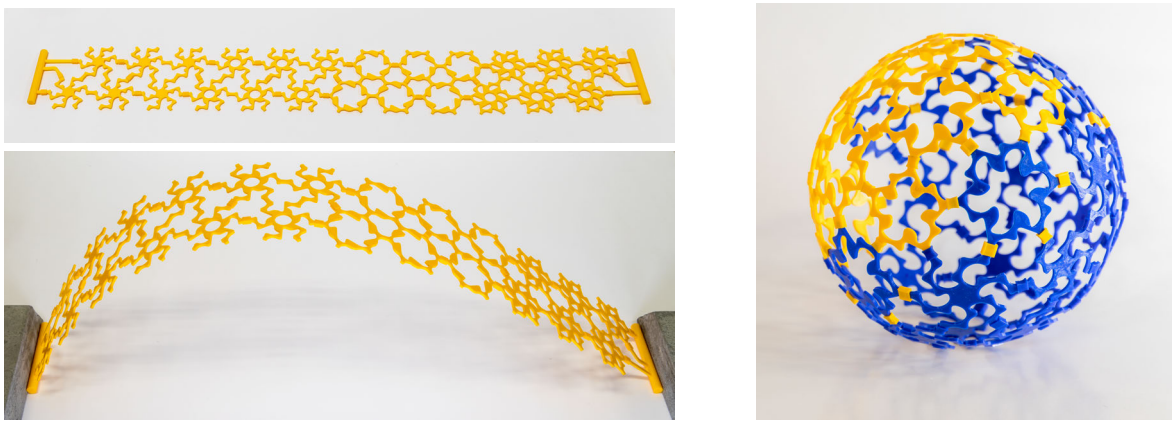

**Figure 15:** *Two fabricated examples to demonstrate the applicability of our method. (Left) a "graded" strip composed of four increasingly stiffer patterns (from left to right): when compressed horizontally the strip bends asymmetrically, accordingly with the employed pattern distribution. (Right) a spherical assembly obtained by tessellating a truncated icosahedron using two patterns.*

sphere is a major strength, as it demonstrates that the present work can be extended to a complete pipeline for inverse design, in which the user provides a generic shape, and the most appropriate patterns are automatically designed/selected so that, once bent and assembled, they match the input shape.

## 6. Conclusions

This work focused on the creation of a family of flat, tileable mechanical metamaterials. Assuming a target surface approximated as a polygon mesh with (almost) regular faces, we defined a regular recursive subdivision of polygons to produce exchangeable patterns to tile the surface. We defined a strategy to filter the disconnected ones, and conditions to ensure tileability. To produce geometries that are both fabricable and suited for simulations, we introduced a proper filleting strategy around non-manifold vertices, along with vertices that produce sharp angles, which could cause singularities in computation during mechanical simulations, and vertices that lie on the polygon boundary. We performed mechanical simulations of each patterns under three loading scenarios, and produce a browsing interface that supports the exploration of the library in terms of aesthetics and mechanical behavior. Overall a great variability in aesthetics and mechanical behaviour is produced. Finally, we demonstrated that our patterns can be fabricated and assembled to create surface tessellations with different out-of-plane bending behavior. Our results demonstrated the feasibility of our method as the first step in the direct design pipeline.

Besides addressing the direct design pipeline, future work could also include the inverse design problem, where an appropriate subset of patterns is designed for a given target shape. A major issue is that metamaterial structures present a complex geometry at the meso-scale, considerably increasing simulation costs. This is the reason that pushed other researchers to work on simplified models, e.g. homogenization, thus severely limiting the design space. A possible research direction for finding equivalent metamaterial properties could be based on artificial intelligence techniques, with learned responses replacing computationally-intensive, physically-based simulations of the generic patterned surfaces.

Finally, a limitation of our approach is that it relies on an a-posteriori filtering procedure of the generated patterns. For the future, we plan to study space-pruning strategies based on topological constraints which allow filtering at each step of recursion. This would orient the combinatorial exploration of the space of patterns towards a family of geometries that meet the constraints from the earlier steps.

## Acknowledgements

This work was partially supported by the NextGenerationEU programme under the funding schemes PNRR-PE-AI scheme (M4C2, investment 1.3, line on AI) FAIR (Future Artificial Intelligence Research).

## References

[BBO*10] BICKEL B., BÄCHER M., OTADUY M. A., LEE H. R., PFISTER H., GROSS M., MATUSIK W.: Design and fabrication of materials with desired deformation behavior. *ACM Transactions on Graphics (TOG) 29*, 4 (2010), 1–10.

[BCMP18] BICKEL B., CIGNONI P., MALOMO L., PIETRONI N.: State of the art on stylized fabrication. *Computer Graphics Forum 37* (02 2018). doi:10.1111/cgf.13327.

[BSP19] BARCHIESI E., SPAGNUOLO M., PLACIDI L.: Mechanical metamaterials: a state of the art. *Mathematics and Mechanics of Solids 24*, 1 (2019), 212–234.

[CML*17] CHEN W., MA Y., LEFEBVRE S., XIN S., MARTÍNEZ J., WANG W.: Fabricable tile decors. *ACM Trans. Graph. 36*, 6 (nov 2017). URL: https://doi.org/10.1145/3130800.3130817, doi:10.1145/3130800.3130817.

[DLL*15] DUMAS J., LU A., LEFEBVRE S., WU J., DICK C.: By-example synthesis of structurally sound patterns. *ACM Trans. Graph. 34*, 4 (jul 2015). URL: https://doi.org/10.1145/2766984, doi:10.1145/2766984.

[GS87] GRUNBAUM B., SHEPHARD G.: Tilings and patterns. w. h, 1987.

[HDD*93] HOPPE H., DEROSE T., DUCHAMP T., MCDONALD J., STUETZLE W.: Mesh optimization. In *Proceedings of the 20th Annual Conference on Computer Graphics and Interactive Techniques* (New York, NY, USA, 1993), SIGGRAPH '93, Association for Computing Machinery, p. 19–26. URL: https://doi.org/10.1145/166117.166119, doi:10.1145/166117.166119.

[HMvdW*20] HARRIS C. R., MILLMAN K. J., VAN DER WALT S. J., GOMMERS R., VIRTANEN P., COURNAPEAU D., WIESER E., TAYLOR J., BERG S., SMITH N. J., KERN R., PICUS M., HOYER S., VAN KERKWIJK M. H., BRETT M., HALDANE A., DEL RÍO J. F., WIEBE M., PETERSON P., GÉRARD-MARCHANT P., SHEPPARD K., REDDY T., WECKESSER W., ABBASI H., GOHLKE C., OLIPHANT T. E.: Array programming with NumPy. *Nature 585*, 7825 (Sept. 2020), 357–362. URL: https://doi.org/10.1038/s41586-020-2649-2, doi:10.1038/s41586-020-2649-2.

[JP*18] JACOBSON A., PANOZZO D., ET AL.: libigl: A simple C++ geometry processing library, 2018. https://libigl.github.io/.

[Kap09] KAPLAN C. S.: Introductory tiling theory for computer graphics. *Synthesis Lectures on Computer Graphics and Animation 4*, 1 (2009), 1–113.

[KMOD09] KHAREVYCH L., MULLEN P., OWHADI H., DESBRUN M.: Numerical coarsening of inhomogeneous elastic materials. *ACM Trans. Graph. 28*, 3 (jul 2009). URL: https://doi.org/10.1145/1531326.1531357, doi:10.1145/1531326.1531357.

[LMC*22] LACCONE F., MALOMO L., CALLIERI M., ALDERIGHI T., MUNTONI A., PONCHIO F., PIETRONI N., CIGNONI P.: Design and construction of a bending-active plywood structure: The flexmaps pavilion. *Journal of the International Association for Shell and Spatial Structures 63*, 2 (2022), 98–114.

[LMP*21] LACCONE F., MALOMO L., PIETRONI N., CIGNONI P., SCHORK T.: Integrated computational framework for the design and fabrication of bending-active structures made from flat sheet material. *Structures 34* (2021), 979–994. URL: https://www.sciencedirect.com/science/article/pii/S2352012421007165, doi:https://doi.org/10.1016/j.istruc.2021.08.004.

[MDLW15] MARTÍNEZ J., DUMAS J., LEFEBVRE S., WEI L.-Y.: Structure and appearance optimization for controllable shape design. *ACM Trans. Graph. 34*, 6 (oct 2015). URL: https://doi.org/10.1145/2816795.2818101, doi:10.1145/2816795.2818101.

[MLC*22] MANOLAS I., LACCONE F., CHERCHI G., MALOMO L., CIGNONI P.: Automated generation of flat tileable patterns and 3D reduced model simulation. *Computers & Graphics 106* (2022), 141–151. URL: https://www.sciencedirect.com/science/article/pii/S0097849322000929, doi:https://doi.org/10.1016/j.cag.2022.05.020.

[MPI*18] MALOMO L., PÉREZ J., IARUSSI E., PIETRONI N., MIGUEL E., CIGNONI P., BICKEL B.: Flexmaps: Computational design of flat flexible shells for shaping 3d objects. *ACM Trans. Graph. 37*, 6 (dec 2018). URL: https://doi.org/10.1145/3272127.3275076, doi:10.1145/3272127.3275076.

[MSS*19] MARTÍNEZ J., SKOURAS M., SCHUMACHER C., HORNUS S., LEFEBVRE S., THOMASZEWSKI B.: Star-shaped metrics for mechanical metamaterial design. *ACM Transactions on Graphics (TOG) 38*, 4 (2019), 1–13.

[PTP*15] PIETRONI N., TONELLI D., PUPPO E., FROLI M., SCOPIGNO R., CIGNONI P.: Statics aware grid shells. *Computer Graphics Forum 34*, 2 (2015), 627–641.

[PZM*15] PANETTA J., ZHOU Q., MALOMO L., PIETRONI N., CIGNONI P., ZORIN D.: Elastic textures for additive fabrication. *ACM Transactions on Graphics (TOG) 34*, 4 (2015), 1–12.

[Seb] SEBASTIAN KOCH: meshplot. URL: https://github.com/skoch9/meshplot.

[ŠJ15] ŠÍR Z., JÜTTLER B.: On de casteljau-type algorithms for rational bézier curves. *Journal of Computational and Applied Mathematics 288* (2015), 244–250.

[SM13] SIGMUND O., MAUTE K.: Topology optimization approaches: A comparative review. *Structural and multidisciplinary optimization 48*, 6 (2013), 1031–1055. doi:https://doi.org/10.1007/s00158-013-0978-6.

[SMGT18] SCHUMACHER C., MARSCHNER S., GROSS M., THOMASZEWSKI B.: Mechanical characterization of structured sheet materials. *ACM Transactions on Graphics (TOG) 37*, 4 (2018), 1–15.

[Smi09] SMITH M.: *ABAQUS/Standard User's Manual, Version 6.9*. Dassault Systèmes Simulia Corp, United States, 2009.

[TDJ*20] TOZONI D. C., DUMAS J., JIANG Z., PANETTA J., PANOZZO D., ZORIN D.: A low-parametric rhombic microstructure family for irregular lattices. *ACM Trans. Graph. 39*, 4 (jul 2020). URL: https://doi.org/10.1145/3386569.3392451, doi:10.1145/3386569.3392451.

[YZL*18] YU X., ZHOU J., LIANG H., JIANG Z., WU L.: Mechanical metamaterials associated with stiffness, rigidity and compressibility: A brief review. *Progress in Materials Science 94* (2018), 114–173.

[ZCT16] ZEHNDER J., COROS S., THOMASZEWSKI B.: Designing structurally-sound ornamental curve networks. *ACM Trans. Graph. 35*, 4 (jul 2016). URL: https://doi.org/10.1145/2897824.2925888, doi:10.1145/2897824.2925888.

[ZJL14] ZHOU S., JIANG C., LEFEBVRE S.: Topology-constrained synthesis of vector patterns. *ACM Trans. Graph. 33*, 6 (nov 2014). URL: https://doi.org/10.1145/2661229.2661238, doi:10.1145/2661229.2661238.